Selective Gas Uptake and Rotational Dynamics in a (3,24)-Connected Metal-Organic Framework Material

William J. F. Trenholme,[a,b] Daniil I. Kolokolov,[c,d] Michelle Bound,[b] Stephen P. Argent,[b] Jamie A. Gould,[b,g] Jiangnan Li,[a] Sarah A. Barnett,[e] Alexander J. Blake,[b] Alexander G. Stepanov,[c,d] Elena Besley,[b] Timothy L. Easun,[b,f] Sihai Yang,*[a] and Martin Schröder*[a]

a. School of Chemistry, University of Manchester, Oxford Rd, Manchester, M13 9PL, U.K
b. School of Chemistry, University of Nottingham, University Park, Nottingham NG7 2RD, U.K.
c. Boreskov Institute of Catalysis, Siberian Branch of Russian Academy of Sciences, Prospekt Akademika Lavrentieva 5, Novosibirsk 630090, Russia
d. Novosibirsk State University, Pirogova Street 2, Novosibirsk 630090, Russia.
e. Diamond Light Source, Harwell Science and Innovation Campus, Didcot, Oxfordshire OX11 0DE, UK.
f. School of Chemistry, Cardiff University, Park Place, Cardiff, CF10 3AT, U.K.
g. Faculty of Science, Agriculture and Engineering, Newcastle University, Newcastle upon Tyne, NE1 7RU, U.K.

ABSTRACT: The desolvated (3,24)-connected metal-organic framework (MOF) material, MFM-160a, $[Cu_3(L)(H_2O)_3]$ [H_6L = 1,3,5-triazine-2,4,6-tris(aminophenyl-4-isophthalic acid)] exhibits excellent high pressure uptake of CO_2 (110 wt% at 20 bar, 298 K) and highly selective separation of C_2 hydrocarbons from CH_4 at 1 bar pressure. Henry's law selectivities of 79:1 for C_2H_2:CH_4 and 70:1 for C_2H_4:CH_4 at 298 K are observed, consistent with IAST predictions. Significantly, MFM-160a shows a selectivity of 16:1 for C_2H_2:CO_2. Solid state ^{2}H NMR spectroscopic studies on partially deuterated MFM-160-d_{12} shows an ultra-low barrier to rotation of the phenyl group in the activated MOF (~2 kJ mol^{-1}), and a rotation rate five orders of magnitude slower than usually observed for solid state materials (1.4 x 10^6 Hz *cf.* 10^{11} - 10^{13} Hz). Upon introduction of CO_2 and C_2H_2 into desolvated MFM-160a, this rate of rotation was found to increase with increasing gas pressure, a phenomenon attributed to the weakening of an intramolecular hydrogen bond in the triazine-containing linker upon gas binding. DFT calculations of binding energies and interactions of CO_2 and C_2H_2 around the triazine-core are entirely consistent with the ^{2}H NMR spectroscopic observations.

INTRODUCTION

Over the past two decades there has been a great deal of interest in metal-organic framework (MOF) materials capable of selectively storing and separating gases. Two areas of significant interest are the capture of CO_2[1–8] and the separation of C_2 hydrocarbons from methane.[9–15] CO_2 is well-established as a leading contributor to climate change and over 85% of the world's energy demand involves the burning of fossil fuels.[16,17] Materials capable of storing CO_2 from flue gas and automobiles are therefore in high demand. The use of MOFs containing polar functional groups such as amines and amides has proven to be effective for the uptake of CO_2 at low pressure, whilst MOFs with very large surface areas have shown exceptional storage capacity for CO_2 at higher pressures.[5,18–21]

Natural gas is a vitally important fuel and is also a feedstock for production of a variety of chemicals.[22] Comprising mainly of CH_4, it is also increasingly being utilized in vehicles as its high H:C ratio results in lowered emissions of CO and CO_2 compared to normal hydrocarbon fuels.[22] The main sources of impurity in natural gas are the C_2 hydrocarbons, C_2H_2, C_2H_4 and C_2H_6.[11] Removing these hydrocarbons increases the purity of natural gas and provides a source of C_2 hydrocarbons for further use.[23,24] Purification and separation of C_2 hydrocarbons are usually achieved by cryogenic distillation, a very energy intensive process, and the use of selective adsorbents to separate different components at room temperature is a potential alternative.[23,24]

We report herein the synthesis of the hexacarboxylate linker H_6L which has been used to prepare a (3,24)-connected Cu(II) material (denoted MFM-160; MFM = Manchester Framework Material) designed for both high CO_2 uptake and selective sorption of C_2 hydrocarbons over CH_4. With this in mind, our ligand design was based around a triazine core,[11,23–26] coupled with a triangular arrangement of three pendant isophthalic acid moieties, which can combine with a Cu(II) paddlewheel motif to give a framework of **rht** topology, used by us[27–32] and others[33–35] to prepare MOFs with exceptional gas storage capacity. We show here that MFM-160 has the potential for extremely high CO_2 uptake at higher pressures, whilst at lower pressures it is capable of highly selective sorption of C_2 hydrocarbons over CH_4 and CO_2.

EXPERIMENTAL

The preparation of H_6L was achieved *via* microwave-assisted nucleophilic substitution between 4-bromoaniline and cyanuric chloride to give the tribromo intermediate (Scheme 1).[36] A microwave-assisted Pd(II) catalyzed Suzuki cross-coupling of this intermediate with 3,5-di(ethoxycarbonyl)phenylboronic acid gave the hexa-ester product, which was then hydrolyzed in aqueous NaOH followed by exceptionally rapid, facile and energy-efficient route to this linker. Solvothermal reaction of H_6L and $Cu(NO_3)_2{\cdot}3H_2O$ in acidified DMF at 80 °C for 24 h yielded green octahedral single crystals of MFM-160, $[Cu_3(L)(H_2O)_3]{\cdot}13DMF{\cdot}7H_2O$.

Density functional theory (DFT) calculations were performed, as implemented in the Q-Chem quantum chemistry package.[37] The strength of adsorption sites was analyzed using a fragment of the linker formed by the central triazine ring and three phenyl rings (Figure S33). The binding energies (BE) between the guest molecule and the linker were calculated in addition to their relative positions corresponding to the strongest binding. These calculations were performed in two stages. Geometry optimization was carried out using dispersion-corrected DFT calculations at the B3LYP/6-31+G** level of theory and the binding energies were subsequently calculated at the higher B3LYP/6-311+G** level with BE = E_{opt}(complex) – E_{opt}(linker) – E_{opt}(guest molecule). Binding energies were corrected for basis set superposition error (BSSE).

Synthesis of H_6L (Scheme 1)

Cyanuric chloride (736 mg, 3.99 mmol) was added to a mixture of 4-bromoaniline (2.20 g, 12.8 mmol, 3.2 eq.) and $NaHCO_3$ (1.08 g, 12.8 mmol, 3.2 eq.) in 1,4-dioxane/DMF (3:1, 30 ml) and the mixture heated at 120 °C in a microwave reactor for 1 h. The solvent was removed under vacuum and the remaining solid was washed with water (2 x 20 ml) and extracted into Et_2O. The organic layer was separated, the solvent removed under vacuum, and the resulting white solid was recrystallized from warm hexane:EtOAc (5:1), filtered and dried to give 2,4,6-tris(4-bromophenylamino)-1,3,5-triazine (1.95 g, 83%). ^{1}H NMR spectroscopy (400 MHz, dmso-d_6) δ = 9.54 (s, 3H), 7.80 (d, 6H, J = 6.8 Hz), 7.46 (d, 6H, J = 8.8 Hz); ^{13}C{^{1}H} NMR (100 MHz, dmso-d_6) δ = 164.3, 139.7, 131.6, 122.7, 114.2.

2,4,6-Tris(4-bromophenylamino)-1,3,5-triazine (1.32 g, 2.23 mmol), diethylisophthalate-5-boronic acid (2.14 g, 8.05 mmol, 3.6 eq.) and K_3PO_4 (8.50 g, 40.1 mmol, 18 eq.) were added to a degassed mixture of 1,4-dioxane/water (10:1, 110 ml). $[Pd(dppf)Cl_2]$ (40 mg, 0.055 mmol, 2.4 % eq.) was added and the reaction heated in a microwave reactor at 85 °C for 1 h. The solvent was removed under vacuum and the product extracted into $CHCl_3$. The combined organic phase was then washed with water and brine and dried over $MgSO_4$. Upon evaporation of $CHCl_3$ the crude product was dissolved in CH_2Cl_2 and purified by passing through a plug of silica gel to give the pure ester product 1,3,5-triazine-2,4,6-tris(aminophenyl-4-isophthalic ethyl ester) as a white solid (1.86 g, 82%). ^{1}H NMR spectroscopy (300 MHz, dmso-d_6) δ = 9.58 (s, 3H), 8.42 (t, 3H, J = 1.5 Hz), 8.39 (d, 6H, J = 1.5 Hz), 8.04 (d, 6H, J = 6.0 Hz), 7.71 (d, 6H, J = 8.7 Hz), 4.37 (q, 12H, J = 7.1 Hz), 1.35 (t, 18H, J = 7.1 Hz); ^{13}C{^{1}H} NMR (100 MHz, dmso-d_6) δ = 165.8, 165.1, 139.6, 138.6, 131.9, 131.5, 130.1, 129.8, 127.5, 121.4, 61.6, 14.6.

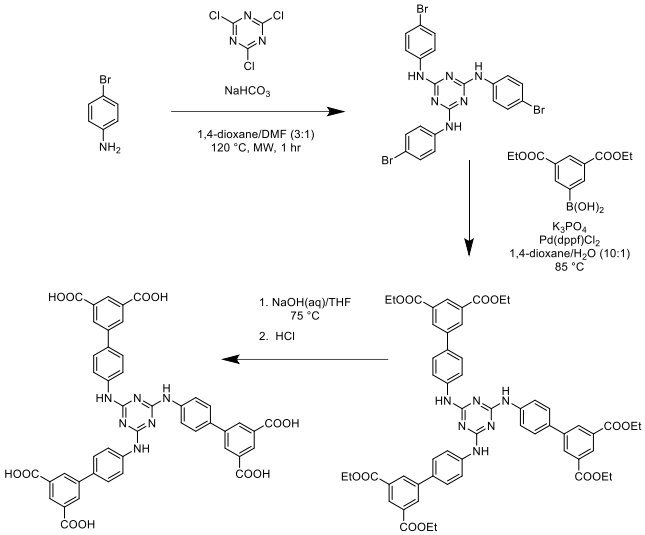

Scheme 1. Synthesis of H_6L.

The hexaester (1.70 g, 1.67 mmol) was dissolved in a mixture of THF (30 ml) and 2M NaOH (30 ml) and heated at 75 °C for 16 h. Upon cooling, THF (30 ml) was added, the aqueous layer was separated and concentrated HCl was added dropwise to the solution until pH ~ 1. The resulting precipitate was filtered and recrystallized from a mixture of hot DMF/water (5:1) to give the H_6L [1,3,5-triazine-2,4,6-tris(aminophenyl-4-isophthalic acid)] as a white solid (1.36 g, 96%). ^{1}H NMR (400 MHz, dmso-d_6) δ = 9.59 (s, 3H), 8.44 (t, 3H, J = 1.6 Hz), 8.39 (d, 6H, J = 1.6 Hz), 8.04 (d, 6H, J = 8.0 Hz), 7.73 (d, 6H, J = 8.8 Hz); ^{13}C{^{1}H} NMR (100 MHz, dmso-d_6) δ = 167.1, 164.5, 141.4, 140.8, 132.6, 132.4, 131.3, 128.7, 127.5, 121.2. Anal. Calcd (Found) for $C_{45}H_{30}N_6O_{12}$: C, 63.83 (63.39); H, 3.57 (3.45); N, 9.93 (9.80)%.

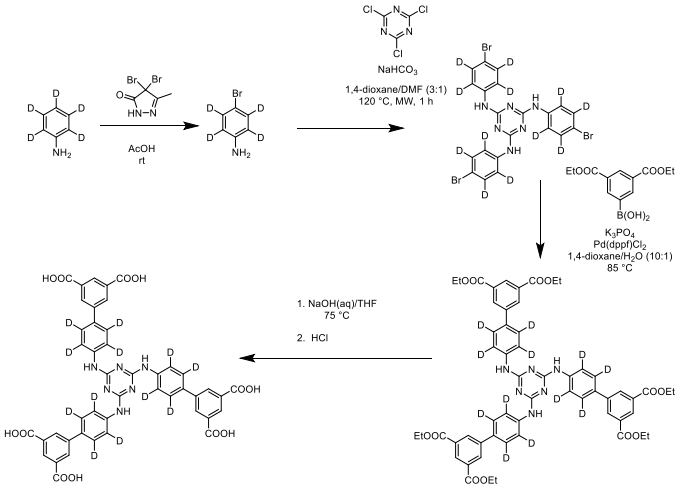

Scheme 2: Synthesis of H_6L-d_{12}.

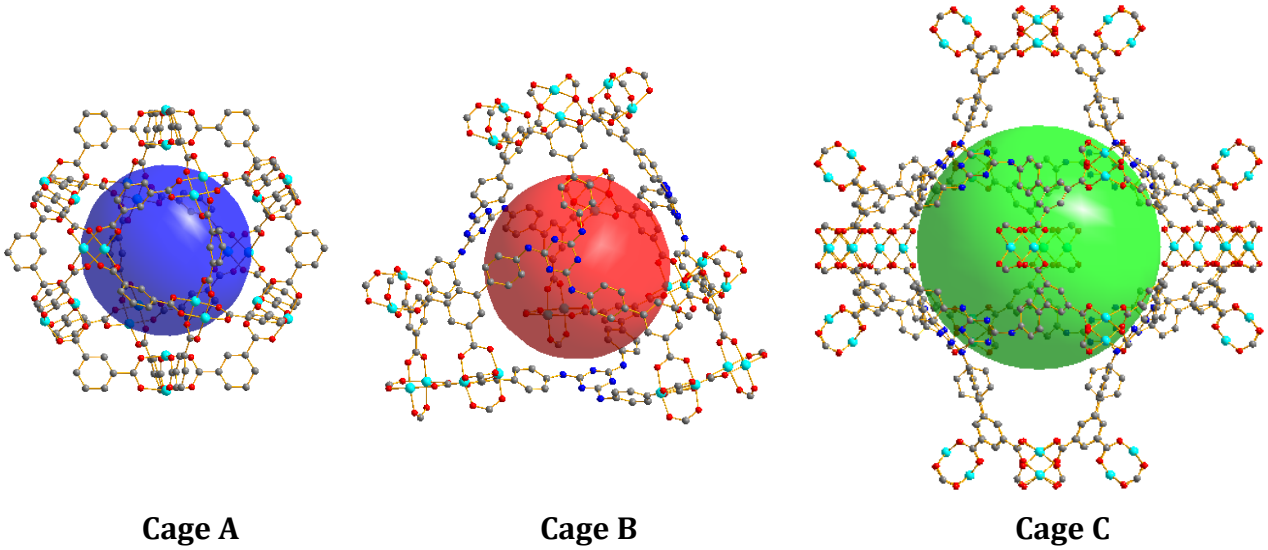

Figure 1. View of cages A, B and C in MFM-160; the large coloured spheres in the centre of the cages represent the solvent accessible volume. Cu: cyan, O: red, N: blue, C: grey. Hydrogen atoms are omitted for clarity.

Synthesis of MFM-160·13DMF·7H_2O

H_6L (100 mg, 0.118 mmol) and $Cu(NO_3)_2{\cdot}3H_2O$ (114 mg, 0.472 mmol, 4 eq.) were added to DMF/H_2O (8 ml; 15:1, v/v) and sonicated until dissolution. A solution of 3M HNO_3 in DMF (3 ml) was then added and the solution heated in a 50 ml Schott bottle at 80 °C for 20 h. The crystalline product was removed by filtration, washed with copious hot DMF and dried to yield a green powder (210 mg, 82 %) Anal. Calcd (Found) for $C_{84}H_{135}N_{19}O_{35}Cu_3$: C, 46.67 (46.28); H, 6.29 (6.23); N, 12.31 (12.42)%. Single crystals of MFM-160 was prepared on a small scale using 20 mg of H_6L and 4 equivalents of $Cu(NO_3)_2{\cdot}3H_2O$ dissolved in DMF (1.5 ml). Addition of 3M HNO_3 in DMF (0.6 ml) followed by heating in a sealed vial at 80 °C for 20 h produced green octahedral crystals suitable for single crystal X-ray diffraction. The syntheses of H_6L-d_{12} and MFM-160-d_{12} (Scheme 2) are described in Supporting Information.

RESULTS AND DISCUSSIONS

MFM-160 crystallizes in the tetragonal space group $I4/m$ with unit cell dimensions a = 32.6838(3) Å, c = 48.0624(7) Å and V = 51341(1) Å^3 and shows a (3,24)-connected framework structure of **rht** topology containing three distinct cages, A, B and C (Figure 1). Cage A is a truncated cuboctahedron formed from 12 [$Cu_2(O_2CR)_4$] paddlewheel units connected to 24 different linkers. With the spacing between cuboctahedra determined by the distance between isophthalate moieties on the arms of the linker. This results in the formation of larger cages B (truncated tetrahedron) and C (truncated cube). With the aqua ligands removed from the axial positions of the paddlewheel, the accessible internal diameter of cage A is 13.0 Å, and of cage B it is 13.8 Å with a cage length of 22.7 Å with the accessible windows between these cages measuring 6.5–8.2 Å. The largest cage, C, has an accessible diameter of 19.6 Å and a cage length of 35.2 Å, with windows of 6.4–8.4 Å. All internal diameters were calculated by fitting a sphere from the center of the cage to its walls, taking into account van der Waals radii. Window diameters were calculated from the largest sphere able to fit through the aperture. The potential accessible volume of desolvated MFM-160a ("a" denotes the desolvated form) is 77% as calculated by the VOID algorithm within the software PLATON[38] (after removal of all guest solvates and coordinated water molecules), with a calculated crystal density of 0.540 g cm^{-3}. Thermogravimetric analysis of the as-synthesized sample of MFM-160 in air showed loss of DMF and H_2O solvent below 170 °C, with the material stable up to 290 °C, above which a mass loss corresponding to framework decomposition is observed (Figure S2).

To prepare activated MFM-160a for gas sorption experiments, the DMF of the as-synthesized sample was exchanged with analytical grade acetone by decanting the mother liquor and replacing with analytical grade acetone. This process was repeated twice daily for 5 days. The sample was then activated by heating at 100 °C under reduced pressure for 20 h, whereupon a color change from dark green to purple was observed; this is a typical indicator of the removal of coordinated solvent from the Cu(II) paddlewheel node. The permanent porosity of the framework was confirmed *via* an N_2 sorption isotherm measured volumetrically at 77 K which showed reversible type-I behavior and an uptake of 983 cm^3 g^{-1} (123 wt%) at 1 bar (Figure S5). The slight changes in gradient in the range 30–120 mbar are assigned to the sequential filling of the micropores and mesopores. The estimated Braun-Emmett-Teller (BET) surface area of MFM-160a as calculated from this isotherm was 3847 m^2 g^{-1}, with a total pore volume of 1.52 cm^3 g^{-1}.

CO_2, H_2 and hydrocarbon gas adsorption isotherms

In order to probe the effectiveness of MFM-160a to adsorb different gases, we performed gas adsorption isotherm experiments between 0–20 bar using CO_2 and CH_4 (298 K and 273 K, Figure 2), and H_2 (77 K and 87 K, Figure S6). Low pressure (0-1 bar) isotherms of C_2 hydrocarbons were run at 273 K and 298 K for comparison with the data obtained for CH_4 (Figure 3).

MFM-160a shows exceptional capacity for CO_2 storage at 20 bar with uptakes of 558 $cm^3\ g^{-1}$ (110 wt%) and 719 $cm^3\ g^{-1}$ (141 wt%) at 298 K and 273 K, respectively. At 195 K and 1 bar MFM-160a nears saturation at 881 $cm^3\ g^{-1}$ (173 wt%). This uptake of CO_2 up to 20 bar at 298 K is one of the highest reported to date: to the best of our knowledge the current record uptake under these conditions is 627 $cm^3\ g^{-1}$ (123 wt%, 19.8 bar) in MOF-177.[5,20] The CH_4 uptake of MFM-160a at 20 bar was 199 $cm^3\ g^{-1}$ (14.2 wt%) at 298 K and 274 $cm^3\ g^{-1}$ (19.6 wt%) at 273 K. The H_2 uptake at 20 bar was 6.4 wt% at 77 K and 5.3 wt % at 87 K, whereas the uptake at 1 bar was 2.14 wt% at 77 K and 1.40 wt% at 87 K (Figure S6).

As shown in Figure 3, the uptakes of C_2H_2, C_2H_4 and C_2H_6 at 273 K are 212 $cm^3\ g^{-1}$ (24.7 wt%), 175 $cm^3\ g^{-1}$ (21.9 wt%) and 201 $cm^3\ g^{-1}$ (27.0 wt%) at 1 bar, respectively. At 298 K these values become 128 $cm^3\ g^{-1}$ (14.9 wt%), 115 $cm^3\ g^{-1}$ (14.4 wt%) and 110 $cm^3\ g^{-1}$ (14.8 wt%). This comparatively extremely low uptake of CH_4 at 1 bar (15.3 $cm^3\ g^{-1}$ at 298 K, 27.1 $cm^3\ g^{-1}$ at 273 K) in MFM-160a makes the material of great interest for selective separation of C_2 hydrocarbons over CH_4. To estimate the selectivity of each hydrocarbon over CH_4 we employed Henry's law, in which constants (K_H) were determined using a virial fit of the measured isotherm data (Figures S7-S16).

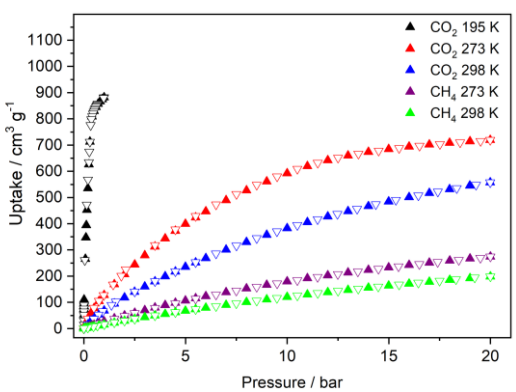

Figure 2. Adsorption isotherms for CO_2 and CH_4 in MFM-160a from 0-20 bar (filled triangles: adsorption; open triangles: desorption).

Using these constants, the selectivity (S) of one gas, *i*, over the second gas, *j*, was determined from the equation:

$$S_{ij} = K_{Hi}/K_{Hj}$$

The selectivities for C_2H_2:CH_4, C_2H_4:CH_4 and C_2H_6:CH_4 at 273 K were calculated to be 104:1, 130:1 and 10:1 respectively. While lower than current benchmark materials such as NKMOF-1-Ni[39] and ZJU-74a[40], the C_2H_2:CH_4 separation of 79:1 at 298 K is comparable to other Cu(II) triazine-based MOFs such as $[Cu_3(TDPAT)]$[11] ($TDPAT^{6-}$ = 2,4,6-tris(3,5-dicarboxylphenylamino)-1,3,5-triazine) and $[Cu_3(TDPAH)]$[23] ($TDPAH^{6-}$ = 2,5,8-tris(3,5-dicarboxylphenylamino)-*s*-heptazine) which have selectivities of 127:1 and 81:1, respectively. However, the calculated selectivities are higher than those reported for smaller-pore Cu(II) MOFs such as UTSA-50a[13] and UTSA-15a[41] (68:1 and 56:1 respectively).

The selectivity for C_2H_2 over CO_2 (15:1 at 298 K; 16:1 at 273 K) demonstrates the potential of MFM-160a for the purification of acetylene, in which CO_2 is a common impurity. A study by Li *et al.*[42] strongly suggested that the presence of N-centers within pores does not improve selectivity for C_2H_2 over CO_2. Thus, in the case of MFM-160a, we tentatively attributed this selectivity to the greater van der Waals interactions between the framework and C_2H_2 molecules, as described by Samsonenko and co-workers for selective uptake of C_2H_2 over CO_2 in porous formates.[43] The separation of CO_2 from C_2H_2 is notoriously difficult as a result of their similar size and sublimation points,[44] and the current high selectivity for C_2H_2 over CO_2 is a promising and represents one of the highest selectivities for a metal-organic framework for this separation.[45,46] It should be noted that repeating the desorption-adsorption cycles of these isotherms gives identical results, confirming the stability of MFM-160 to repeated activation and re-use.

In addition to Henry's law, the gas selectivities for C_2H_2:CH_4, C_2H_4:CH_4, C_2H_6:CH_4 and C_2H_2:CO_2 in binary mixtures were analyzed using the IAST model.[47] Each isotherm was fitted using a dual-site or single-site Langmuir-Freundlich model with the chosen model based on the accuracy of the resulting fitting (Figures S17-26). The selectivities for each mixture (Figure 3c and S27) are in agreement with the Henry's law calculations at 273 K, as the order of selectivity over CH_4 is shown to be C_2H_4 > C_2H_2 >> C_2H_6. At very low pressures (~20 mbar) the C_2H_4:CH_4 selectivity is predicted to be 110:1, which decreases rapidly with increasing pressure before reaching 26:1 at 1 bar. The C_2H_2:CH_4 selectivity is 97:1 below 30 mbar and decreases to 28:1 at 1 bar. At 298 K the IAST predictions show that the selectivity for C_2H_4 over CH_4 is much greater than that of C_2H_2 between 20 and 200 mbar (111:1 *versus* 51:1 at 20 mbar), although the selectivities are approximately equal at 1 bar.

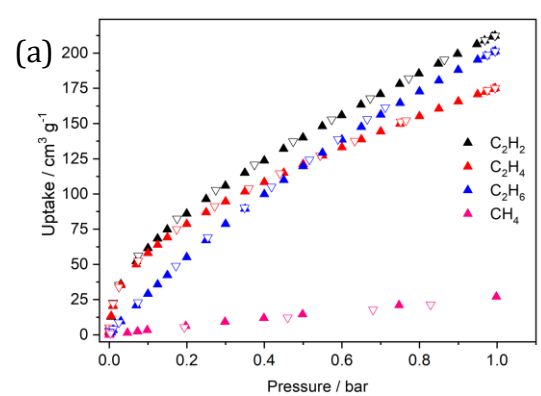

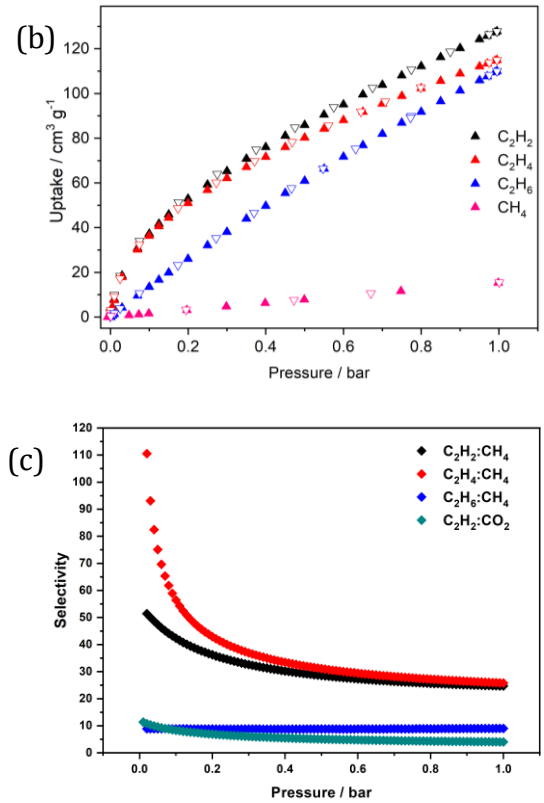

Figure 3. Adsorption isotherms for CH_4, C_2H_6, C_2H_4 and C_2H_2 in MFM-160a from 0-1 bar at (a) 273 K, (b) at 298 K (filled triangles: adsorption; open triangles: desorption), and (c) calculated IAST selectivities for MFM-160a at 298 K.

The isosteric heats of adsorption (Q_{st}) for each gas were calculated using a virial method to fit the sorption isotherms at 273 K and 298 K. The heats of adsorption at zero-loading for CO_2, C_2H_2, C_2H_4 and C_2H_6 are 30, 37, 36 and 24 kJ mol^{-1}, respectively. Each has a higher Q_{st} at zero-loading than CH_4 (23 kJ mol^{-1}). The values of Q_{st} follow the same pattern as the selectivities at 298 K (C_2H_2 > C_2H_4 >> C_2H_6), although at 273 K the C_2H_4:CH_4 selectivity is greater than the C_2H_2:CH_4 selectivity (130:1 *versus* 104:1).

Solid state ^{2}H NMR spectroscopic studies of activated and gas-loaded MFM-160

In order to gain a greater understanding of the C_2H_2:CO_2 separation and of the behavior of both gases within the porous material, ^{2}H NMR spectroscopic studies were carried out on a partially deuterated analogue of MFM-160, denoted MFM-160-d_{12} (Scheme 2). The dynamics of the phenyl ring can affect the adsorption properties in two ways: firstly, the phenyl rings themselves provide an accessible adsorption site as a result of the aromatic π-system; secondly, the phenyl rotation directly affects the effective size and geometry of the pore. Probing the framework dynamics is also of interest for comparison with other known MOFs, thus improving understanding of structure-property relationships. The rotational dynamics in MFM-160-d_{12} were probed in the activated, desolvated material (Figures 4 and S28), in the presence of CO_2 at 1 bar and 5 bar loadings (Figure S29 and S30, respectively) and in the presence of C_2H_2 at 0.32 bar and 1 bar (Figure S31 and 32, respectively). As the low pressure uptake of C_2H_2 is significantly higher than that of CO_2, respective pressures of 0.32 and 1 bar were chosen for comparison of the two gases at the same concentrations. The loading of 0.32 bar C_2H_2 and 1 bar of CO_2 each correspond to ~3.1 gas molecules per linker, where the empirical formula of MFM-160-d_{12} gives a density of 1043.43 g mol^{-1}. The higher loadings of 1 bar C_2H_2 and 5 bar CO_2 correspond to 5.9 and 10.8 molecules per linker, respectively.

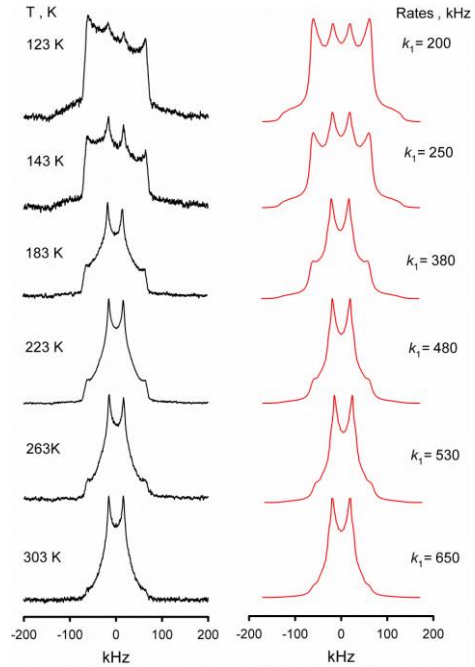

Figure 4. Temperature dependence of the line shape of resonances due to the phenyl groups in guest-free MFM-160-d_{12} as measured by ^{2}H NMR spectroscopy (experimental, black; simulation, red).

In the activated, desolvated MFM-160-d_{12} the temperature-dependent behavior of the line shapes in the ^{2}H NMR spectra confirms that the deuterated phenyl rings are mobile, with a dynamic process gradually developing between ~ 120 K and 300 K (Figures 4 and 5). Below 123 K the line shape is mainly composed of a Pake-powder pattern with quadrupolar coupling parameters (Q_0 = 176 kHz, η_0 ~ 0) typical for a static C-D group on the ^{2}H NMR spectroscopic timescale. At ~ 300 K, the spectrum is dominated by the narrowed line-shape expected for an axial rotation around the phenyl C_2 axis (Q_1 ~20 kHz ~ Q_0/8).[48] At the same time, over the whole temperature range studied, these two components co-exist. Such a phenomenon has been reported for UiO-66[49] and indicates that the phenyl motion at each given temperature is characterized by a distribution of rotation rates, which suggests that the rotational potential fluctuates to a certain degree across the framework. In common with work by Schmidt *et al.*,[50] the rate constant is assumed to obey a log-normal distribution with k_1 being the mean value of the rotation rate at each give temperature and σ being the width of the distribution. By considering the C_2 symmetry of the phenyl fragment, the uniaxial rotation around the C_2 axis can be modeled either by a 4-site or a 6-site jump rotation

model (Figure 6). Notably, in most cases the 6-site jump model can efficiently describe also more complex axial rotations.[51] Numerical fitting of the experimentally observed ^{2}H NMR spectroscopic patterns shows that only the 6-site jump rotation gives an agreement with our data.

Although the distribution of the jump sites has to obey C_2 symmetry, the initial position of the phenyl orientation might be distorted from a fully symmetric case. This distortion is readily introduced into the re-orientation model as an angular parameter φ_i (Figure 6). For a 6-site jump rotation mechanism the jump positions are given as follows: $\varphi_1 = \varphi_i$, $\varphi_2 = \pi/2$, $\varphi_3 = \pi - \varphi_1$, $\varphi_4 = \pi + \varphi_1$, $\varphi_5 = \pi/2$, $\varphi_6 = \pi + \varphi_2$. Within such a model we assume that all positions have equal probability. In our model, the angle $\varphi_i = 45^\circ$, where φ_i is the angle between the plane of the mobile phenyl ring and the plane of the aromatic ring fixed to the Cu(II) node. Thus, it follows that the value $\Delta\varphi_1 = 2\varphi_i$ can be directly compared with the crystal structure. Despite the model being able to give distinct rate constants for each elementary jump, we have found that a simple kinetic matrix defined by one rate constant is sufficient to provide good agreement with the experimental observations. Thus, this 6-site jump rotation model accurately simulates the experimental temperature dependence of the ^{2}H NMR spectral line shapes. The model $\Delta\varphi_1 = 2\varphi_i \sim 90^\circ$ is consistent with the crystallographic data and underscores that the orientation of the phenyl rings is not homogeneously distributed. The log-normal distribution width is almost constant over the temperature range and is $\sigma \sim 1.3$-1.4. Thus, the present inhomogeneity is considerably lower than that observed in UiO-66 and may be attributed to the flexible nature of MFM-160.

The most striking features of the ^{2}H NMR spectra for MFM-160-d_{12} are the kinetic parameters of the deuterated phenyl motion: the Arrhenius plot (Figure 7a) is linear and shows an activation barrier, E_0 = 2.1 kJ mol^{-1} and collision factor, $k_{00}/2\pi$ = 1.4 x 10^6 Hz. This activation barrier is so low that it is comparable to the torsional barrier for methyl groups in xylenes or 2-methylimidazole, *i.e.* aromatic systems where the internal steric interactions are minimized. The torsional barrier for methyl groups in such compounds has been measured experimentally by neutron scattering techniques and ^{2}H NMR spectroscopy which confirm in both cases that E_0 does not exceed 1.5 kJ mol^{-1}.[52,53] Such low values have not been reported previously for solid state materials based upon carboxylate ligands and have been confirmed for many different samples of MFM-160-d_{12}. However, similar low barriers have been reported recently for MOFs incorporating metal-amine linkers such as 2-methylimidazole in ZIF-8[52] and dabco in [Zn_2(bdc)$_2$(dabco)].[54]

It is interesting to consider the possible sources of steric interaction hindering phenyl rotation in MFM-160-d_{12}. The electrostatic interactions are maximized when all aromatic rings are in the same plane, in which case the closest interatomic distances can be given as $d_1 \sim 2.2$ Å, $d_2 \sim 3.1$ Å and $d_3 \sim 2.0$ Å (Figure 8). The main interaction is likely governed by sites III and I, but these distances do not offer an obvious explanation for the ultra-low value of k_{00} (usually $\sim 10^{11\text{-}13}$ Hz in MOF materials)

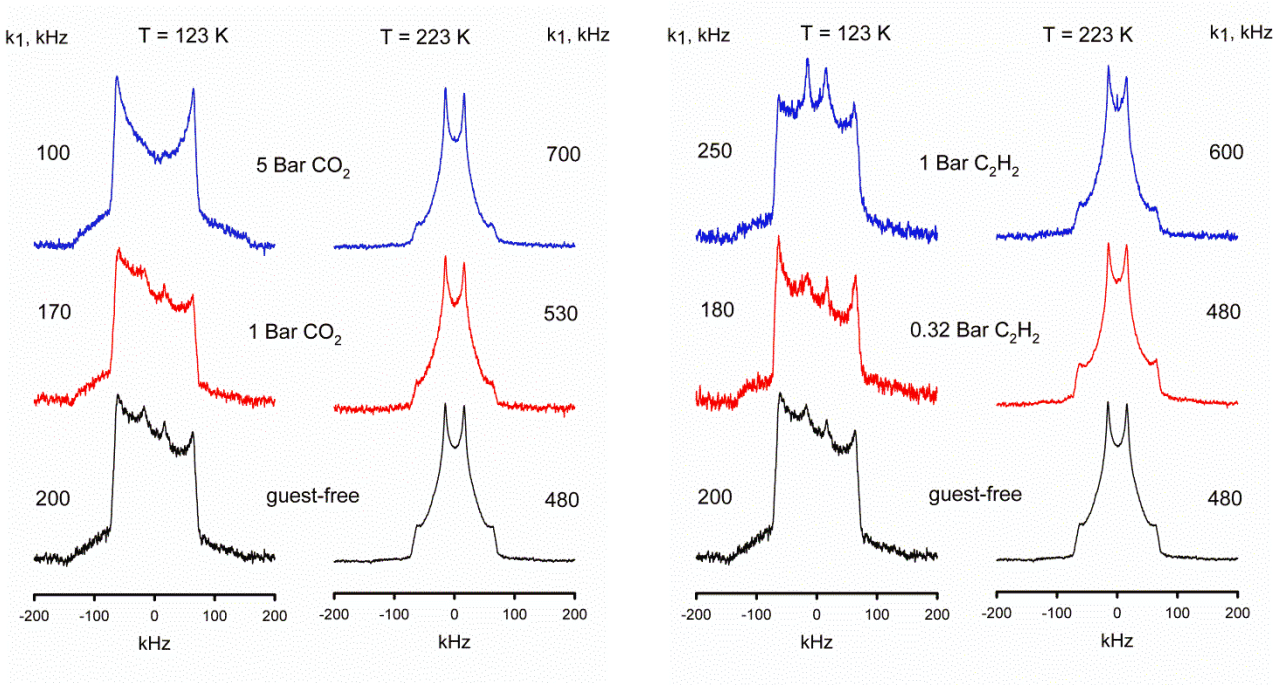

Figure 5. Comparison of the experimental line shapes and rotation rates for phenyl groups in guest-loaded MFM-160-d$_{12}$ at 123 K and 223 K.

However, this may be explained by the short intramolecular hydrogen bond (1.91 Å) between the phenyl protons and the triazine N atoms observed in the crystal structure, thus restricting the rotation of the ring by affecting its pre-exponential factor.

Although the effect of gas-loading is not very strong in terms of absolute values, it is an unexpected one (Figure 5). With CO_2 as the guest species, the concentration dependence at 123 K is as expected with a higher gas loading resulting in a slower rate of phenyl rotation. At the higher loading of ~5 bar (at 298 K), the decrease in rotation rate is more pronounced and evident even without detailed numerical analysis of the observed line shape. However, at 223 K this effect is inverted: with increased loading of CO_2, the rate of phenyl rotation actually *increases*, a phenomenon previously unobserved in a MOF or any other solid state material.[55] On a quantitative level the effect is clearly seen on an Arrhenius plot (Figure 7b) for the corresponding rotational rate constants: the slope for the CO_2-loaded material is notably steeper in comparison to that of the guest-free material. While not very pronounced for the intermediate loading (1 bar) with E_1 = 2.6 kJ mol^{-1}, $k_{10}/2\pi$ = 2.3 x 10^6 Hz, the effect becomes more evident at higher concentration (5 bar) with E_2 = 4.2 kJ mol^{-1}, $k_{20}/2\pi$ = 7.6 x 10^6 Hz. In the latter case the barrier is approximately doubled compared with the desolvated material, but the collision factor is increased by six-fold, so even though the barrier has increased the collision factor overrides this suggesting that CO_2 blocks or breaks the internal H-bonding, thus allowing more rapid rotation of the phenyl groups. It is possible to readily observe the collision factor behavior because of the extremely low starting value for the guest-free material, i.e. $k_{00}/2\pi$ =1.4 x 10^6 Hz, while normal pre-exponential factors for an elementary rotation are typically in the range of 10$^{11-13}$ Hz.

For the C_2H_2-loaded material, the situation is different: at the intermediate concentration (~0.32 bar at RT), conditions in which the C_2H_2 concentration is equimolar to that of CO_2 at 1 bar, no effect on the phenyl dynamics is observed (Figure 7c) and the rotation is characterized by the same parameters as for the activated, desolvated MFM-160-d_{12} with E_3 = 1.9 kJ mol^{-1} and k_{30} =1.2 x 10^6 Hz. Upon increasing C_2H_2 concentration to 1 bar, the rate of phenyl ring rotation clearly increases, however the activation barrier remains the same E_4 = 1.9 kJ mol^{-1} but the collision factor rises to k_{40} =1.8 x 10^6 Hz. This is shown on the corresponding Arrhenius plots (Figure 7c).

This behavior can be interpreted in terms of host-guest interactions. At the lower loading the phenyl rings do not interact with C_2H_2 and only at higher loadings is there a subtle increase of the collision factor. This shows that occupancy of C_2H_2 sites around the mobile phenyl rings is low, even at higher concentrations. Thus, C_2H_2 coordinates predominantly to the Cu(II) paddlewheel sites and interacts with the phenyl rings only through random collisions, most likely when most of the metal sites are occupied. At 0.32 bar C_2H_2 (3.1 gas molecules per formula unit) the Cu(II) sites are very likely saturated with C_2H_2 bound strongly and not able to influence phenyl rotation, as shown by ^{2}H NMR spectroscopy.

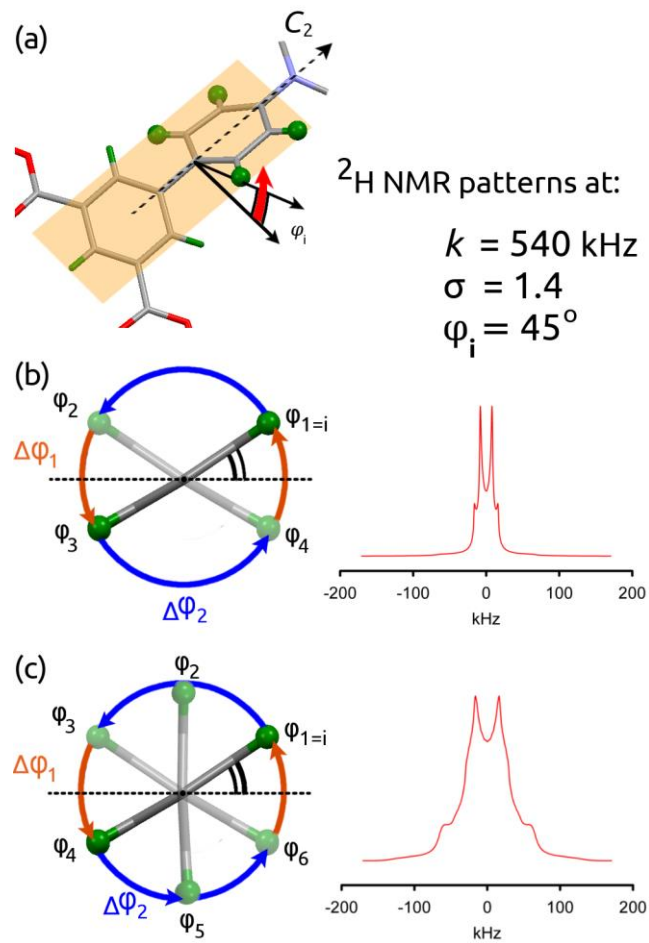

Figure 6. View of stable orientation sites for the phenyl rings depending on the jump rotation model: (a) the starting position of the plane of the mobile phenyl ring is tilted by an angle φ_i. The axial jump-rotation about the C_2 symmetry axis of the phenyl group is then realised by either (b), an n = 4 site exchange motion, or by (c) an n = 6 site exchange. The distribution of the orientation sites is governed only by the value of the first position $\varphi_1 = \varphi_i$. All elementary jumps are assumed to be governed by the same rate constant $k = k_1/n$. Even in the case of the same value of φ_i in the intermediate jump rate the two models give qualitatively distinct patterns.

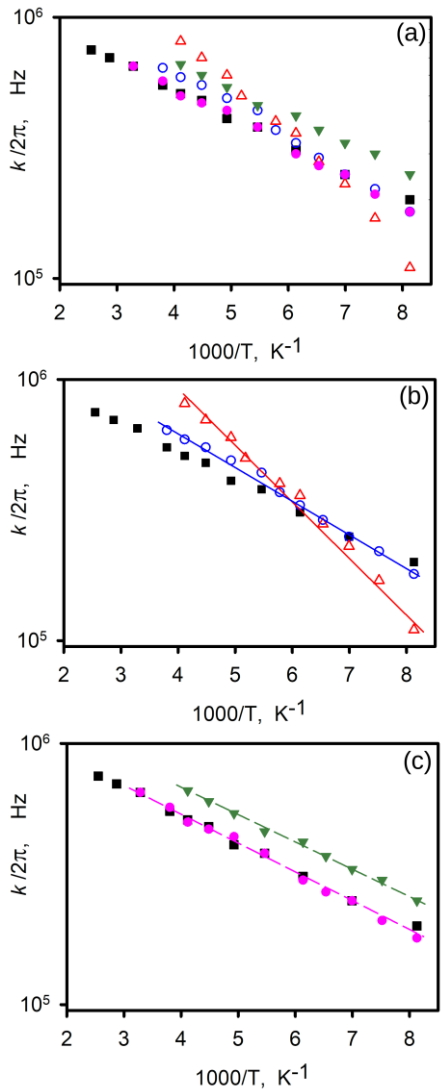

Figure 7. Arrhenius plots of the rotation rate constants k_1. a) Arrhenius plot of all gas-loaded samples b) Arrhenius plot of CO_2-loaded MFM-160 c) Arrhenius plot of C_2H_2-loaded MFM-160 (■) guest-free MFM-160-d_{12}; (blue-○) 1 bar CO_2 loading; (red-Δ) 5 bar CO_2 loading; (pink-●) 0.32 bar C_2H_2 loading; (dark green-▼) 1 bar C_2H_2 loading. All gas loadings were performed at 298 K.

However, with an equimolar loading of CO_2, where the Cu(II) sites were also expected to be saturated, the phenyl ring rotation is much more affected by the guest CO_2 molecules than for C_2H_2, strongly suggesting that CO_2 occupies binding sites on the linker, while open Cu(II) sites are still available. These observations, therefore, provide a good insight into the selectivity for C_2H_2 over CO_2, as the stronger binding of C_2H_2 at the open Cu(II) sites very likely accounts for the greater uptake of C_2H_2 at low pressures. Interestingly, the C_2H_2:CO_2 selectivity in [Cu_2(pzdc)$_2$(pyz)] (pzdc^{2-} = pyrazine-2,3-dicarboxylate; pyz = pyrazine), a MOF without open Cu(II) sites, was assigned to the binding of C_2H_2 with free carboxylate oxygen atoms lining the pores.[56]

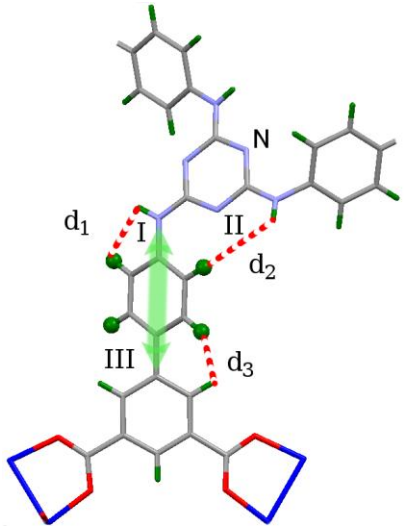

Figure 8. View of the deuterated (green) mobile phenyl ring in MFM-160-d_{12}. The scheme shows the possible hydrogen bonding sites (I, II, and III) that will influence the rotational potential for rotation of the phenyl group.

Computational modelling of gas binding sites in MFM-160

To understand further the observations from ^{2}H NMR spectroscopy and to help explain the hydrocarbon selectivity demonstrated by MFM-160, DFT calculations were performed using the Q-Chem quantum chemistry package.[37]

An extensive search for binding sites between all guest molecules and the linker fragment was performed, with configurations showing the strongest binding and binding energy ranges summarized in Tables 1; Table S2 shows the full range of binding configurations. The strongest binding of CO_2 to the linker fragment was found to be at site A1 (Table 1), in which the CO_2 molecule interacts above the linker with a binding energy of –19.5 kJ mol^{-1}. The interaction is dominated by a strong electrostatic interaction between the carbon of CO_2 and the N-center of the central ring. This interaction is enhanced by two weak hydrogen bonds between the other oxygen of CO_2 and nearby protons of the neighboring phenyl ring and the bridging –NH group. These interactions have a significant cooperative effect on the binding of CO_2 to the linker fragment. The slow rotation of the phenyl ring as observed by ^{2}H NMR spectroscopy was attributed to a hydrogen bond between a phenyl proton and an N atom of triazine core. Therefore, the increased rotation upon CO_2 loading may be explained by the weakening or removal of this hydrogen bond upon CO_2 binding at site A1. Increased occupancy of gas at this site at higher CO_2 loading would also explain the increased rate of rotation from the 1 bar to the 5 bar-loaded sample. Overall, CO_2 interacts more strongly with the linker fragment than C_2H_2, giving a range of binding energies from –19.5 to –12.4 kJ mol^{-1}.

The strongest binding site for C_2H_2 is over the bridging amine nitrogen between the triazine ring and the outer phenyl rings with a binding energy of –18.2 kJ mol^{-1} (site C1, Table 1). There is a cooperative binding effect with the hydrogens of the C_2H_2 interacting with the triazine ring and the

neighboring phenyl ring, but the binding is dominated by an interaction between the π-bonds of the C_2H_2 and the bridging nitrogen. As with CO_2, this interaction is likely to affect the hydrogen bond between the phenyl proton and the triazine core, leading to the increased phenyl rotation rate observed by ^2H NMR spectroscopy upon addition of 1 bar C_2H_2. At lower pressures (0 to 0.32 bar), this site is unoccupied, as confirmed by the values of E_0 and k_{00} at 0.32 bar remaining the same as those observed in the guest-free material. Between 0.32 and 1 bar, where the Cu(II) paddlewheel sites are expected to be saturated, the increased occupancy of this site disrupts the intramolecular hydrogen bond of the linker and the phenyl rotation increases. It would have been interesting to observe the effect of a higher loading of C_2H_2 on the rotational dynamics, but there are well-established safety concerns with the use of C_2H_2 above 1 bar.

The π-bond interaction of C_2H_2 with the linker leads to stronger interactions overall compared to other hydrocarbons, and as a result the C_2H_2 molecule interacts with a similar range of binding energies as CO_2 (–13.3 to –18.2 kJ mol^{-1}). These comparable binding energies strongly suggest that the triazine functionality is not responsible for the selectivity for C_2H_2 over CO_2. As stated earlier, it is likely that increased van der Waals interactions between C_2H_2 and the framework in comparison to those with CO_2, as well as the higher affinity of the former for the open Cu(II) sites, are responsible for the selective uptake.

The range of interactions between the hydrocarbons C_2H_4 and C_2H_6 and the linker were also investigated and found to be very similar; –11.7 to –16.2 kJ mol^{-1} and –10.2 to –16.3 kJ mol^{-1} respectively. The strongest interaction between C_2H_4 and the linker and also C_2H_6 and the linker occurs over the central triazine ring. This is an interaction between the central carbon-carbon bond of the two hydrocarbons, C_2H_4 and C_2H_6 and the delocalized π system of the central ring. On average, the binding of C_2H_4 is stronger than C_2H_6 due to the strength of the interaction between the alkene double bond and the linker.

Table 1. The optimised B3LYP/B3LYP/6-31+G* and B3LYP/6-311+G* binding energies and structural details of $C_{21}H_{18}N_6$–guest molecule complexes corresponding to these strongest binding energies

Guests	Optimised geometry	Parameters
CO_2	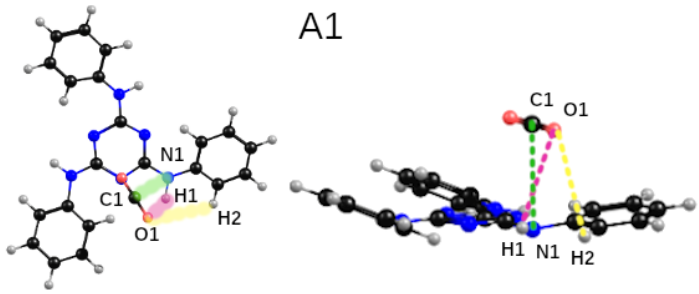	Binding energy: ΔE = – 19.5 kJ mol^{-1} Distance C–N1···C1 (CO_2): 3.25 Å Distance N–H1···O1 (CO_2): 3.00 Å Distance C–H2···O1 (CO_2): 2.98 Å Angle ∠C–N1···C1 (CO_2): 104.63° Angle ∠N1–H1···O1 (CO_2): 103.39° Angle ∠C–H2···O1 (CO_2): 129.12,°
CH_4	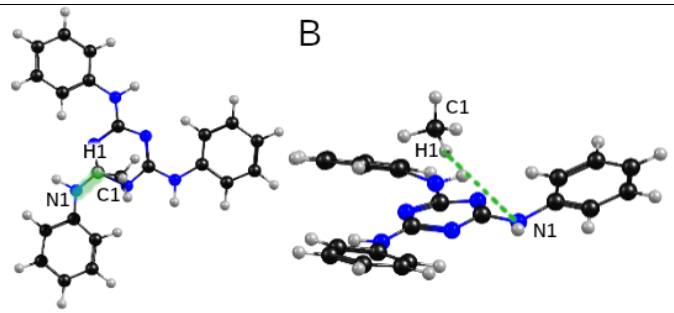	Binding energy: ΔE = – 10.3 kJ mol^{-1} Distance C–N1···H1 (CH_4): 2.97 Å Distance (C_3N_3)···H (CH_4): 3.32 Å Angle ∠C–N1···H1 (CH_4): 93.79° Angle ∠ring···C1 (CH_4): 100.02°

C_2H_2	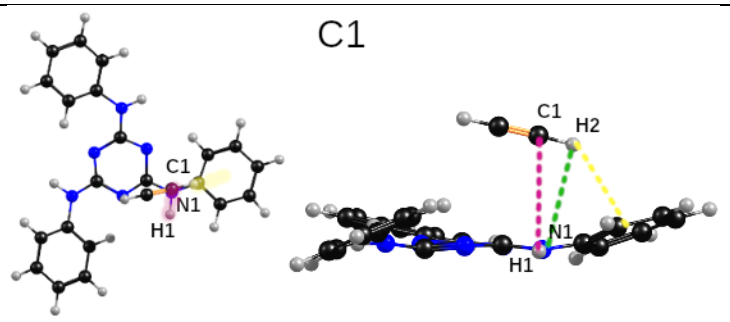	Binding energy: $\Delta E = -18.2$ kJ mol^{-1} Distance H–N1···C1 (C_2H_2): 3.35 Å Distance C–N1···H2 (C_2H_2): 3.70 Å Distance (C_6H_5)···H2 (C_2H_2): 2.28 Å Angle ∠H–N1···C1(C_2H_2): 98.80° Angle ∠C–N1···H2 (C_2H_2): 93.05° Angle ∠(C_6H_5)···H2 (C_2H_2): 108.73°
C_2H_4	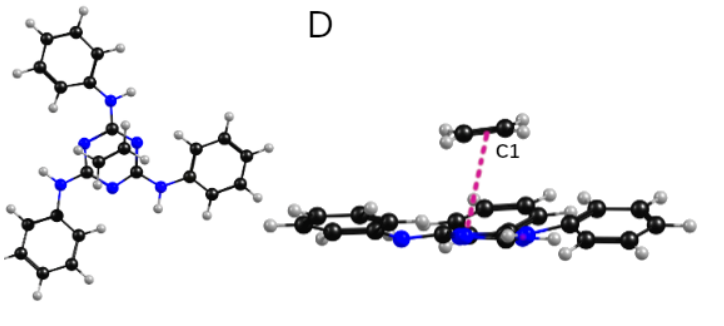	Binding energy: $\Delta E = -16.2$ kJ mol^{-1} Distance (C_3N_3)···(C_2H_4): 3.33 Å Angle ∠(C_3N_3)···C1(C_2H_4): 78.47°
C_2H_6	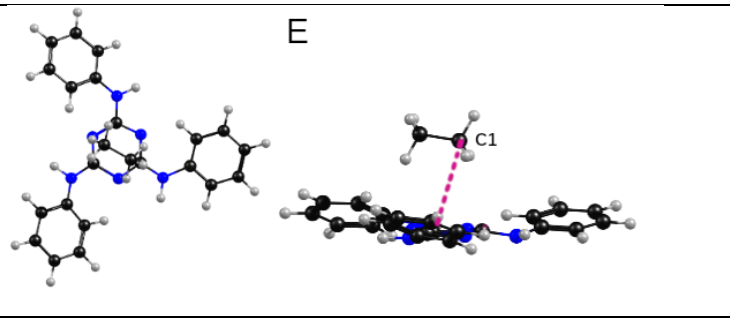	Binding energy: $\Delta E = -16.3$kJ mol^{-1} Distance (C_3N_3)···(C_2H_6): 3.55 Å Angle ∠(C_3N_3)···C1(C_2H_6): 75.95°

To complete the computational investigation, we found that the strongest binding of CH_4 to the linker was found to be in complex B (Table 1) where the CH_4 molecule interacts above the central triazine ring to give a binding energy of –10.3 kJ mol^{-1}. There is a weak hydrogen bond between a CH_4 hydrogen atom and a nitrogen atom of the triazine ring. There are also additional weak electrostatic interactions between other CH_4 hydrogen atoms and the central ring. The binding energy interactions between CH_4 and the linker are the weakest of all those studied, consistent with the experimental isotherm data.

CONCLUSIONS

In conclusion, we have demonstrated an energy and cost-efficient route to a large hexacarboxylate linker through microwave-assisted synthesis. This led to the synthesis of a new, highly porous (3,24)-connected Cu(II) MOF, designated MFM-160. We have shown that its activated form MFM-160a exhibits an exceptional capacity for uptake of CO_2 at 20 bar and 298K (110 wt%). We have also shown that the relatively poor uptake of CO_2 and CH_4 at lower pressures (≤ 1 bar) makes MFM-160a a material of interest for the purification of natural gas and of acetylene, as confirmed by Henry's Law and IAST calculations. A ^{2}H NMR spectroscopic study of phenyl rotation dynamics confirmed an ultra-low rotation barrier, but very slow phenyl rotation. The rotation was shown to increase upon gas loading, a unique phenomenon not previously observed in a solid state material and is attributed to an intramolecular hydrogen bond, which is weakened by gas binding, leading to an increased rate of rotation. The results of DFT calculations are consistent with this, as both gases show clear binding interactions near this hydrogen bond.

ASSOCIATED CONTENT

Supporting Information: Experimental details and supporting cif files, additional figures, graphs, and tables. This material is available free of charge via the Internet at http://pubs.acs.org.

AUTHOR INFORMATION

Corresponding Author

*Sihai.Yang@nottingham.ac.uk, *M.Schroder@nottingham.ac.uk

Author Contributions

The manuscript was written through contributions of all authors.

Notes

The authors declare no competing financial interest.

ACKNOWLEDGMENT

We thank the EPSRC, the University of Nottingham and the University of Manchester for funding. This project has received funding to M.S. from the European Research Council (ERC) under the European Union's Horizon 2020 research and innovation programme (grant agreement No 742401, *NANOCHEM*). We are very grateful to Diamond Light Source for access to Beamline I19. WJFT thanks Johnson Matthey for funding and Dr Hugh Hamilton and Dr Ian Casely for valuable discussions. TLE gratefully acknowledges the Royal Society for the award of a University Research Fellowship. MS and DIK gratefully acknowledge receipt of the Royal Society International Exchanges Scheme grant ref. IE150114. DIK also acknowledges the support from the Russian Science Foundation, project 17-73-10135. DIK and AGS also acknowledge the support of Ministry of Science and High Education of the Russian Federation (Project no. AAAA-A17-117041710084-2). EB and MB acknowledge the High Performance Computing (HPC) Facility at the University of Nottingham for providing computational time. JL also thanks China Scholarship Council (CSC) for funding.

REFERENCES

(1) Chen, K. J.; Scott, H. S.; Madden, D. G.; Pham, T.; Kumar, A.; Bajpai, A.; Lusi, M.; Forrest, K. A.; Space, B.; Perry, J. J.; Zaworotko, M. J. Benchmark C_2H_2/CO_2 and CO_2/C_2H_2 separation by two closely related hybrid ultramicroporous materials. *Chem* **2016**, *1*, 753–765.

(2) Ding, M.; Flaig, R. W.; Jiang, H. L.; Yaghi, O. M. Carbon capture and conversion using metal–organic frameworks and MOF-based materials. *Chem. Soc. Rev.* **2019**, *48*, 2783–2828.

(3) Alsmail, N. H.; Suyetin, M.; Yan, Y.; Cabot, R.; Krap, C. P.; Lü, J.; Easun, T. L.; Bichoutskaia, E.; Lewis, W.; Blake, A. J.; Schröder, M. Analysis of high and selective uptake of CO_2 in an oxamide-containing $\{Cu_2(OOCR)_4\}$-based metal–organic framework. *Chem. - A Eur. J.* **2014**, *20*, 7317–7324.

(4) An, J.; Geib, S. J.; Rosi, N. L. High and selective CO_2 uptake in a cobalt adeninate metal–organic framework exhibiting pyrimidine- and amino-Decorated pores. *J. Am. Chem. Soc.* **2010**, *132*, 38–39.

(5) Millward, A. R.; Yaghi, O. M. Metal–organic frameworks with exceptionally high capacity for storage of carbon dioxide at room temperature. *J. Am. Chem. Soc.* **2005**, *127*, 17998–17999.

(6) Forse, A. C.; Milner, P. J.; Lee, J. H.; Redfearn, H. N.; Oktawiec, J.; Siegelman, R. L.; Martell, J. D.; Dinakar, B.; Porter-Zasada, L. B.; Gonzalez, M. I.; Neaton, J. B.; Long, J. R.; Reimer, J. A. Elucidating CO_2 chemisorption in diamine-appended metal–organic frameworks. *J. Am. Chem. Soc.* **2018**, *140*, 18016–18031.

(7) Yang, S.; Sun, J.; Ramirez-Cuesta, A. J.; Callear, S. K.; David, W. I. F.; Anderson, D. P.; Newby, R.; Blake, A. J.; Parker, J. E.; Tang, C. C.; Schröder, M. Selectivity and Direct visualization of carbon dioxide and sulfur dioxide in a decorated porous host. *Nat. Chem.* **2012**, *4*, 887–894.

(8) Carrington, E. J.; McAnally, C. A.; Fletcher, A. J.; Thompson, S. P.; Warren, M.; Brammer, L. Solvent-switchable continuous-breathing behaviour in a diamondoid metal–organic frameworks and its influence on CO_2 versus CH_4 Selectivity. *Nat. Chem.* **2017**, *9* (9), 882–889.

(9) Yang, L.; Qian, S.; Wang, X.; Cui, X.; Chen, B.; Xing, H. Energy-efficient separation alternatives: metal–organic frameworks and membranes for hydrocarbon separation. *Chem. Soc. Rev.* **2020**, *49*, 5359–5406.

(10) Hu, F.; Di, Z.; Wu, M.; Li, J. Building a robust 3D Ca-MOF by a new square Ca_4O SBU for purification of natural gas. *Dalt. Trans.* **2020**, *49*, 8836–8840.

(11) Liu, K.; Ma, D.; Li, B.; Li, Y.; Yao, K.; Zhang, Z.; Han, Y.; Shi, Z. High storage capacity and separation selectivity for C_2 hydrocarbons over methane in the metal–organic framework Cu–TDPAT. *J. Mater. Chem. A* **2014**, *2*, 15823–15828.

(12) Li, Q.; Wu, N.; Li, J.; Wu, D.; Li, Y. Amino-functionalized water-stable metal–organic framework for enhanced C_2H_2/CH_4 separation performance. *Inorg. Chem.* **2020**, *59*, 2631–2635..

(13) Xu, H.; Cai, J.; Xiang, S.; Zhang, Z.; Wu, C.; Rao, X.; Cui, Y.; Yang, Y.; Krishna, R.; Chen, B.; Qian, G. A cationic microporous metal–organic framework for highly selective separation of small hydrocarbons at room temperature. *J. Mater. Chem. A* **2013**, *1*, 9916–9921.

(14) He, Y.; Song, C.; Ling, Y.; Wu, C.; Krishna, R.; Chen, B. A new MOF-5 homologue for selective separation of methane from C_2 hydrocarbons at room temperature. *APL Mater.* **2014**, *2*, 124102–124106.

(15) Barnett, B. R.; Gonzalez, M. I.; Long, J. R. Recent progress towards light hydrocarbon separations using metal–organic frameworks. *Trends Chem.* **2019**, *1*, 159–171.

(16) Rackley, S. A. *Carbon capture and storage*; Butterworth-Heinemann, 2010.

(17) Li, J.-R.; Ma, Y.; McCarthy, M. C.; Sculley, J.; Yu, J.; Jeong, H.-K.; Balbuena, P. B.; Zhou, H.-C. Carbon dioxide capture-related gas adsorption and separation in metal–organic frameworks. *Coord. Chem. Rev.* **2011**, *255*, 1791–1823.

(18) Zheng, B.; Bai, J.; Duan, J.; Wojtas, L.; Zaworotko, M. J. Enhanced CO_2 binding affinity of a high-uptake rht-type metal–organic framework decorated with acylamide groups. *J. Am. Chem. Soc.* **2011**, *133*, 748–751.

(19) Yuan, D.; Zhao, D.; Sun, D.; Zhou, H.-C. An isoreticular series of metal–organic frameworks with dendritic hexacarboxylate ligands and exceptionally high gas-uptake capacity. *Angew. Chemie Int. Ed.* **2010**, *49*, 5357–5361.

(20) Furukawa, H.; Ko, N.; Go, Y. B.; Aratani, N.; Choi, S. B.; Choi, E.; Yazaydin, A. O.; Snurr, R. Q.; O'Keeffe, M.; Kim, J.; Yaghi, O. M. Ultrahigh porosity in metal–organic frameworks. *Science* **2010**, *329*, 424–428.

(21) Llewellyn, P. L.; Bourrelly, S.; Serre, C.; Vimont, A.; Daturi, M.; Hamon, L.; De Weireld, G.; Chang, J.-S.; Hong, D.-Y.; Kyu Hwang, Y.; Hwa Jhung, S.; Férey, G. High uptakes of CO_2 and CH_4 in mesoporous metal–organic frameworks MIL-100 and MIL-101. *Langmuir* **2008**, *24*, 7245–7250.

(22) Czaja, A. U.; Trukhan, N.; Müller, U. Industrial applications of metal–organic frameworks. *Chem. Soc. Rev.* **2009**, *38*, 1284–1293.

(23) Liu, K.; Li, B.; Li, Y.; Li, X.; Yang, F.; Zeng, G.; Peng, Y.; Zhang, Z.; Li, G.; Shi, Z.; Feng, S.; Song, D. An N-rich metal–organic framework with an rht topology: high CO_2 and C_2 hydrocarbons uptake and selective capture from CH_4. *Chem. Commun.* **2014**, *50*, 5031–5033.

(24) Yang, S.; Ramirez-Cuesta, A. J.; Newby, R.; Garcia-Sakai, V.; Manuel, P.; Callear, S. K.; Campbell, S. I.; Tang, C. C.; Schröder, M. Supramolecular binding and separation of hydrocarbons within a functionalized porous metal–organic framework. *Nat. Chem.* **2015**, *7*, 121–129.

(25) Li, B.; Zhang, Z.; Li, Y.; Yao, K.; Zhu, Y.; Deng, Z.; Yang, F.; Zhou, X.; Li, G.; Wu, H.; Nijem, N.; Chabal, Y. J.; Lai, Z.; Han, Y.; Shi, Z.; Feng, S.; Li, J. Enhanced binding affinity, remarkable selectivity, and high capacity of CO_2 by dual functionalization of a rht-type metal-organic framework. *Angew. Chemie Int. Ed.* **2012**, *51*, 1412–1415.

(26) Luebke, R.; Eubank, J. F.; Cairns, A. J.; Belmabkhout, Y.; Wojtas, L.; Eddaoudi, M. The unique rht-mof platform, ideal for pinpointing the functionalization and CO_2 adsorption relationship. *Chem. Commun.* **2012**, *48*, 1455–1457.

(27) Yan, Y.; Lin, X.; Yang, S.; Blake, A. J.; Dailly, A.; Champness, N. R.; Hubberstey, P.; Schröder, M. Exceptionally high H_2 storage by a

metal–organic polyhedral framework. *Chem. Commun.* **2009**, 1025–1027.
(28) Yan, Y.; Telepeni, I.; Yang, S.; Lin, X.; Kockelmann, W.; Dailly, A.; Blake, A. J.; Lewis, W.; Walker, G. S.; Allan, D. R.; Barnett, S. A.; Champness, N. R.; Schröder, M. Metal-organic polyhedral frameworks: high H_2 adsorption capacities and neutron powder diffraction studies. *J. Am. Chem. Soc.* **2010**, *132*, 4092–4094.
(29) Yan, Y.; Blake, A. J.; Lewis, W.; Barnett, S. A.; Dailly, A.; Champness, N. R.; Schröder, M. Modifying cage structures in metal-organic polyhedral frameworks for H_2 storage. *Chem. - A Eur. J.* **2011**, *17*, 11162–11170.
(30) Yan, Y.; Yang, S.; Blake, A. J.; Lewis, W.; Poirier, E.; Barnett, S. A.; Champness, N. R.; Schröder, M. A mesoporous metal–organic framework constructed from a nanosized C_3-symmetric linker and [Cu_{24}(isophthalate)$_{24}$] cuboctahedra. *Chem. Commun.* **2011**, *47*, 9995–9997.
(31) Yan, Y.; Suyetin, M.; Bichoutskaia, E.; Blake, A. J.; Allan, D. R.; Barnett, S. A.; Schröder, M. Modulating the packing of [Cu_{24}(isophthalate)$_{24}$] cuboctahedra in a triazole-containing metal–organic polyhedral framework. *Chem. Sci.* **2013**, *4*, 1731–1736.
(32) Yan, Y.; Yang, S.; Blake, A. J.; Schröder, M. Studies on metal–organic frameworks of Cu(II) with isophthalate linkers for hydrogen storage. *Acc. Chem. Res.* **2014**, *47*, 296–307.
(33) Farha, O. K.; Özgür Yazaydın, A.; Eryazici, I.; Malliakas, C. D.; Hauser, B. G.; Kanatzidis, M. G.; Nguyen, S. T.; Snurr, R. Q.; Hupp, J. T. De novo synthesis of a metal–organic framework material featuring ultrahigh surface area and gas storage capacities. *Nat. Chem.* **2010**, *2*, 944–948.
(34) Farha, O. K.; Eryazici, I.; Jeong, N. C.; Hauser, B. G.; Wilmer, C. E.; Sarjeant, A. A.; Snurr, R. Q.; Nguyen, S. T.; Yazaydın, A. Ö.; Hupp, J. T. Metal–organic framework materials with ultrahigh surface areas: is the sky the limit? *J. Am. Chem. Soc.* **2012**, *134*, 15016–15021.
(35) Farha, O. K.; Wilmer, C. E.; Eryazici, I.; Hauser, B. G.; Parilla, P. A.; O'Neill, K.; Sarjeant, A. A.; Nguyen, S. T.; Snurr, R. Q.; Hupp, J. T. Designing higher surface area metal–organic frameworks: are triple bonds better than phenyls? *J. Am. Chem. Soc.* **2012**, *134*, 9860–9863.
(36) Sha, Y.; Dong, Y. Microwave assisted synthesis of 2,4,6-triarylamino-1,3,5-triazines as potential UV absorbent. *Synth. Commun.* **2003**, *33*, 2599–2604.
(37) Shao, Y.; Molnar, L. F.; Jung, Y.; Kussmann, J.; Ochsenfeld, C.; Brown, S. T.; Gilbert, A. T. B.; Slipchenko, L. V.; Levchenko, S. V.; O'Neill, D. P.; DiStasio Jr, R. A.; Lochan, R. C.; Wang, T.; Beran, G. J. O.; Besley, N. A.; Herbert, J. M.; Yeh Lin, C.; Van Voorhis, T.; Hung Chien, S.; Sodt, A.; Steele, R. P.; Rassolov, V. A.; Maslen, P. E.; Korambath, P. P.; Adamson, R. D.; Austin, B.; Baker, J.; Byrd, E. F. C.; Dachsel, H.; Doerksen, R. J.; Dreuw, A.; Dunietz, B. D.; Dutoi, A. D.; Furlani, T. R.; Gwaltney, S. R.; Heyden, A.; Hirata, S.; Hsu, C.-P.; Kedziora, G.; Khalliulin, R. Z.; Klunzinger, P.; Lee, A. M.; Lee, M. S.; Liang, W.; Lotan, I.; Nair, N.; Peters, B.; Proynov, E. I.; Pieniazek, P. A.; Min Rhee, Y.; Ritchie, J.; Rosta, E.; David Sherrill, C.; Simmonett, A. C.; Subotnik, J. E.; Lee Woodcock III, H.; Zhang, W.; Bell, A. T.; Chakraborty, A. K.; Chipman, D. M.; Keil, F. J.; Warshel, A.; Hehre, W. J.; Schaefer III, H. F.; Kong, J.; Krylov, A. I.; Gill, P. M. W.; Head-Gordon, M. Advances in methods and algorithms in a modern quantum chemistry program package. *Phys. Chem. Chem. Phys.* **2006**, *8*, 3172–3191.
(37) Spek, A. L. PLATON SQUEEZE: A tool for the calculation of the disordered solvent contribution to the calculated structure factors. *Acta Crystallogr. Sect. C Struct. Chem.* **2015**, *71*, 9–18.
(39) Peng, Y. L.; Pham, T.; Li, P.; Wang, T.; Chen, Y.; Chen, K. J.; Forrest, K. A.; Space, B.; Cheng, P.; Zaworotko, M. J.; Zhang, Z. Robust ultramicroporous metal–organic frameworks with benchmark affinity for acetylene. *Angew. Chemie - Int. Ed.* **2018**, *57*, 10971–10975.
(40) Pei, J.; Shao, K.; Wang, J. X.; Wen, H. M.; Yang, Y.; Cui, Y.; Krishna, R.; Li, B.; Qian, G. A chemically stable Hofmann-type metal–organic framework with sandwich-like binding sites for benchmark acetylene capture. *Adv. Mater.* **2020**, *32*, 1908275.
(41) Chen, Z.; Xiang, S.; Arman, H. D.; Mondal, J. U.; Li, P.; Zhao, D.; Chen, B. Three-dimensional pillar-layered copper(II) metal–organic framework with immobilized functional OH groups on pore surfaces for highly selective CO_2/CH_4 and C_2H_2/CH_4 gas sorption at room temperature. *Inorg. Chem.* **2011**, *50*, 3442–3446.
(42) Li, J.-R.; Tao, Y.; Yu, Q.; Bu, X.-H.; Sakamoto, H.; Kitagawa, S. Selective gas adsorption and unique structural topology of a highly stable guest-free zeolite-type MOF material with N-rich chiral open channels. *Chem. - A Eur. J.* **2008**, *14*, 2771–2776.
(43) Samsonenko, D. G.; Kim, H.; Sun, Y.; Kim, G.-H.; Lee, H.-S.; Kim, K. Microporous magnesium and manganese formates for acetylene storage and separation. *Chem. – An Asian J.* **2007**, *2*, 484–488.
(44) Matsuda, R.; Kitaura, R.; Kitagawa, S.; Kubota, Y.; Belosludov, R. V.; Kobayashi, T. C.; Sakamoto, H.; Chiba, T.; Takata, M.; Kawazoe, Y.; Mita, Y. Highly controlled acetylene accommodation in a metal–organic microporous material. *Nature* **2005**, *436*, 238–241.
(45) Mukherjee, S.; Sensharma, D.; Chen, K.-J.; Zaworotko, M. J. Crystal engineering of porous coordination networks to enable separation of C_2 hydrocarbons. *Chem. Commun.* **2020**, *56*, 10419-10441
(46) Lin, R. B.; Li, L.; Wu, H.; Arman, H.; Li, B.; Lin, R. G.; Zhou, W.; Chen, B. Optimized separation of acetylene from carbon dioxide and ethylene in a microporous material. *J. Am. Chem. Soc.* **2017**, *139*, 8022–8028.
(47) Myers, A. L.; Prausnitz, J. M. Thermodynamics of Mixed-Gas Adsorption. *AIChE J.* **1965**, *11*, 121–127.
(48) Richard A. Komoroski. *High resolution nmr spectroscopy of synthetic polymers in bulk*; VCH Publishers: New York, 1986.
(49) Kolokolov, D. I.; Stepanov, A. G.; Guillerm, V.; Serre, C.; Frick, B.; Jobic, H. Probing the dynamics of the porous Zr terephthalate UiO-66 framework using ^{2}H NMR and neutron scattering. *J. Phys. Chem. C* **2012**, *116*, 12131–12136.
(50) Schmidt, C.; Kuhn, K. J.; Spiess, H. W. Distribution of correlation times in glassy polymers from pulsed deuteron NMR. In *Frontiers in Polymer Science*; Steinkopff: Darmstadt, 1985; Vol. 71, pp 71–76.
(51) Macho, V.; Brombacher, L.; Spiess, H. W. The NMR-WEBLAB: An internet approach to NMR lineshape analysis. *Appl. Magn. Reson.* **2001**, *20*, 405–432.
(52) Kolokolov, D. I.; Stepanov, A. G.; Jobic, H. Mobility of the 2-methylimidazolate linkers in ZIF-8 probed by ^{2}H NMR: saloon doors for the guests. *J. Phys. Chem. C* **2015**, *119*, 27512–27520.
(53) Kirstein, O.; Prager, M.; Dimeo, R. M.; Desmedt, A. Rotational dynamics of methyl groups in m-xylene. *J. Chem. Phys.* **2005**, *122*, 014502.
(54) Gabuda, S. P.; Kozlova, S. G.; Samsonenko, D. G.; Dybtsev, D. N.; Fedin, V. P. Quantum rotations and chiral polarization of qubit prototype molecules in a highly porous metal–organic framework: ^{1}H NMR T_1 study. *J. Phys. Chem. C* **2011**, *115*, 20460–20465.
(55) Khudozhitkov, A. E.; Arzumanov, S. S.; Kolokolov, D. I.; Kholdeeva, O. A.; Freude, D.; Stepanov, A. G. Guests like gear levers: donor binding to coordinatively unsaturated metal sites in MIL-101 controls the linker's rotation. *Chem. - A Eur. J.* **2019**, *25*, 5163–5168.
(56) Zhang, Z.; Xiang, S.; Chen, B. Microporous metal–organic frameworks for acetylene storage and separation. *CrystEngComm* **2011**, *13*, 5983–5992.

TOC